Met. Mater. Int., Vol. 21, No. 5 (2015), pp. 857~864
doi: 10.1007/s12540-015-5044-z

Temperature Dependence of Initial Passivity Breakdown of AZ61 and AZ91D Mg Alloys in 0.1 M NaCl Solution

Yun-Il Choi[1,*], Kensuke Kuroda[2], and Masazumi Okido[2]

[1]Materials Technology Development Team, Corporate R&D Institute, Doosan Heavy Industries & Construction, 22, DoosanVolvo-ro, Seongsan-gu, Changwon, Gyeongnam 642-792, Korea
[2]EcoTopia Science Institute, Nagoya University, Furo-cho, Chikusa-ku, Nagoya 464-8603, Japan

(received date: 19 January 2015 / accepted date: 15 May 2015)

The effects of solution temperature on the initial corrosion characteristics of wrought AZ61 and die-cast AZ91D Mg alloys in 0.1 M NaCl were analyzed. Systematic studies indicate that AZ91D exhibits higher corrosion resistance than AZ61 at room temperature. However, at high temperatures of around 55 °C, we observed contradictory corrosion behavior, as demonstrated by cyclic corrosion tests and electrochemical tests including potentiodynamic polarization, potentiostatic polarization, and elecrochemical impedance spectroscopy. As a result, AZ61 rather showed higher corrosion resistance from the point of view of pit initiation during the immersion at 55 °C resulting from the strengthening of surface passivation. These results can be attributed to the microstructure of AZ61 which contains sub-micron scale β-phase particles dispersed effectively within the α-Mg grains whereas AZ91D has many α-Mg that do not containing any β-phases.

Keywords: magnesium, pitting corrosion, passivity, surface, electrochemistry

1. INTRODUCTION

Magnesium and its alloys have been favored as lightweight solutions in automobile and aerospace industries during past few decades. They are the lightest of all metal alloys, and therefore, are an excellent choice for engineering applications that demand critical weight design considerations. However, Mg is a very active metal, and tends to form a surface layer of corrosion products such as hydroxides and oxides, when in direct contact with water or air. The corrosion susceptibility of Mg alloys depends on the stability of such corrosion products. In particular, the presence of Cl^- degrades their stability in aqueous solutions compared to Al alloys and steels. Only under ideal condition is the corrosion of Mg alloy limited, especially in places that are not exposed to environments containing H_2O and Cl^-. Therefore, under real time conditions, Mg alloys are used as chassis, interiors, and power train, e.g. brake/clutch bracket assemblies, seat bases/risers, ABS housing, steering wheels, and almost all sorts of brackets and housings, wherein corrosion of Mg alloys is avoidable [1].

Consequently, recent research efforts on the development and applications of new Mg alloys have focused on possible ways to decrease their corrosion. Al is the principal alloying element for various Mg alloys, which, when alloyed from 4% up to 10%, significantly impedes the surface corrosion of Mg in active environments [2]. The corrosion of Mg alloys is typically affected by the amount and distribution of intermetallic phases, e.g. $Mg_{17}Al_{12}$ (β-phase). In this context, several studies have analyzed the effects of Al content and the corresponding microstructure on the corrosion behavior of Mg alloys [3-15]. In general, increasing the Al content normally decreases the corrosion susceptibility of Mg alloys. However, some studies have recently reported a contradictory corrosion behavior in Mg-Al type Mg alloys [8-11]. These results act as direct experimental evidences for the theoretical prediction that the β-phase either behave as a barrier for the corrosion or act as a micro-galvanic cathode. The β-phase, which is in a finely and continuously dispersed state, acts as a barrier layer for surface degradation [7]. On the other hand, some authors have claimed that the formation of small and intergranular precipitates of β-phase results in a rapid galvanic corrosion between α-matrix and β-phase [16]. This implies that, even for the same alloy composition, different processing methods can result in Mg alloys with different microstructures, leading to the contradictory corrosion behavior [10,17]. Nevertheless, the effect of Al content and the corresponding specific corrosion mechanism of Mg alloy still remain ambiguous. Much less studies concerning the effect of solution temperature on the corrosion behavior of Mg alloys have been carried out [8].

In this study, we have investigated the effects of electrolyte temperature on the electrochemical properties of wrought

*Corresponding author: yooniri@hotmail.com

AZ61 and die-cast AZ91D. Especially, we have focused on their initial corrosion behavior in 0.1 M NaCl solution and demonstrated the contradicting corrosion behavior between AZ61 and AZ91D at high electrolyte temperature. We cautiously predict that the results obtained in this study may provide guidelines for the methods adopted for processing Mg alloys.

2. EXPERIMENTAL PROCEDURES

Table 1 summarizes the chemical compositions of the different AZ-type Mg alloys (wrought AZ61, die-cast AZ91D) used as test coupons in this study. The Mg alloy sheets were ground up to 2000 grit by using a fine-grained emery paper, ultrasonically cleaned for 3 min in ethanol, and then quickly dried in cool air. The working area of each coupon (1 × 1 cm^2) was limited with hydrophobic adhesive masking tape.

The corrosion characteristics of the Mg alloys were assessed by means of potentiodynamic tests, electrochemical impedance spectroscopy (EIS), and potentiostatic tests in 0.1 M NaCl aqueous solution in the temperature range of 25-55 °C. The potentiodynamic polarization tests were carried out in a potential ranging from -1 to +1 V vs. open circuit potential E_{OCP} after stabilizing E_{OCP} for 30 min. The corresponding currents were recorded at scan rate set to 1 mV s^{-1}. For the EIS measurements, the real and imaginary components of the electrochemical cell were evaluated over a frequency range of 10^5 to 10^{-2} Hz with a amplitude of 10 mV, where the applied potential was -1.38 $V_{Ag/AgCl}$ and E_{OCP}, respectively. The EIS measurements at the E_{OCP} were carried out after an initial open circuit delay of 30 min, and those at -1.38 $V_{Ag/AgCl}$ were carried out immediately after immersion, for all temperatures. The electrochemical cells were fabricated by using Mg alloy sheets under study as the working electrode (WE), a platinum wire as the counter electrode (CE), and Ag/AgCl reference electrode (with saturated KCl) as the reference electrode (RE).

Figure 1 shows the photograph and schematic of the 3-electrode electrochemical cell designed for monitoring the corrosion behavior of Mg alloys in a chamber during the cyclic corrosion tests (CCT). This cell is essentially a modification of the setup reported in previous studies [18,19]. Although the cyclic corrosion testing conditions are very severe for Mg corrosion, it was carried out to adequately simulate complex service conditions usually found in the field.

The cell was constructed by embedding two identical Mg alloys (WEs) in parallel in epoxy at a distance of 6 mm apart, with the RE placed at the center, in between the WEs. Note that it is highly important to maintain electrical contact between these WEs and RE during the entire CCT measurements, especially for the dry stage. When a localized corrosion occurs on one WE at a given test environment, excess electrons flow toward the other WE to cathodically protect its surface [19]. At this moment, the current difference between the two WEs and their mixed potential can be measured by connecting a zero resistance ammeter (ZRA) and a potentiostat. The details of operating cycles and the conditions for each setup of the CCT are described in Table 2.

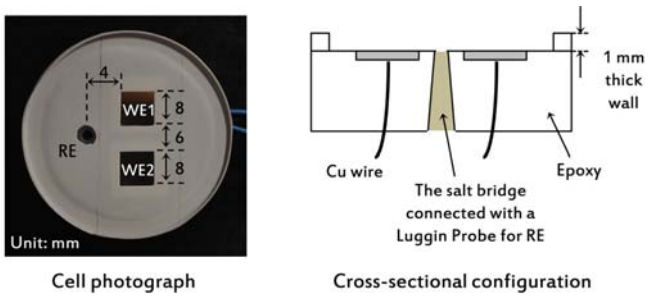

Fig. 1. Photograph and schematic of the electrochemical cell, employing two identical working electrodes, used for corrosion monitoring during cyclic corrosion tests. The WE1 and WE2 connect the working electrode and counter electrode of potentiostat, respectively.

Table 2. Test condition of the cyclic corrosion test (T = operating temperature, RH = relative humidity)

Operating cycles	Conditions of each step
Salt spray (2 h)	5 wt% NaCl, T: 35 °C, RH: 100%
Dry (4 h)	T: 60 °C, RH: 25%
Wet (2 h)	T: 50 °C, RH: 100%

Furthermore, the microstructure of the test specimens was examined by using scanning electron microscopy (SEM). For this, AZ61 and AZ91D were etched for approximately 5 s with 5% Nital (5 mL HNO_3 + 95 mL ethanol) to observe the general constituents [8].

3. RESULTS AND DISCUSSION

3.1. β-phase distribution

The distribution of β-phase as a secondary phase of the Mg alloys was examined by using SEM analysis, as shown in Fig. 2. The precipitation of a relatively thick layer of β-phase at the grain boundaries of α-Mg was observed in AZ91, as compared to AZ61. We could also observe many grains without any β-phase. In case of AZ61, however, the dimen-

Table 1. Chemical compositions (wt%) of the Mg alloys used in this study

	Al	Zn	Mn	Fe	Si	Cu	Ni	Mg
AZ31B	3.29	0.75	0.30	0.03	< 0.01	< 0.01	< 0.01	Bal.
AZ61	5.91	1.16	0.21	< 0.01	0.04	0.04	< 0.01	Bal.
AZ91D	9.12	0.55	0.31	< 0.01	0.02	< 0.001	< 0.001	Bal.

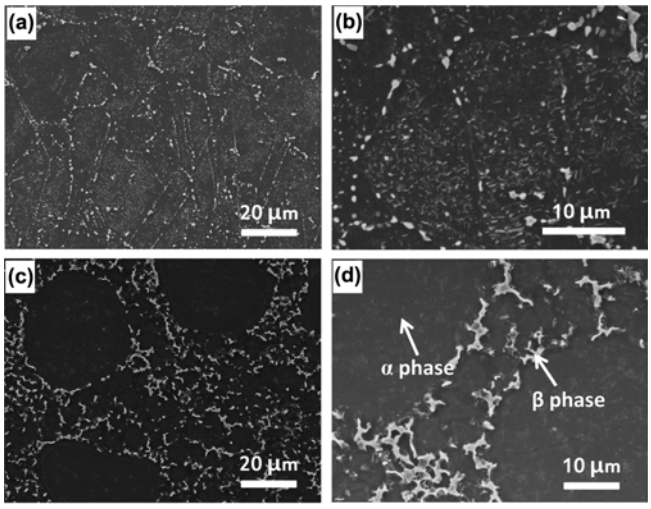

Fig. 2. SEM images of the alloys: (a, b) AZ61 and (c, d) AZ91D.

sion of β-phase at the grain boundaries was approximately half of that of AZ91D. Moreover, sub-micron scale particles of β-phase were being effectively dispersed within the grains (Fig. 2b). For the metastable-stable pit transition, it is mandatory to have a critical pit size or depth at a given corrosive environment [20,21]. Moreover, on Mg alloys, the pitting corrosion is demonstrated to happen mainly on the α-matrix with a segregation of salt particles [4]. These imply that the chances for the growth of active pits beyond the critical size may be more remarkable in case of AZ91D, when compared to AZ61.

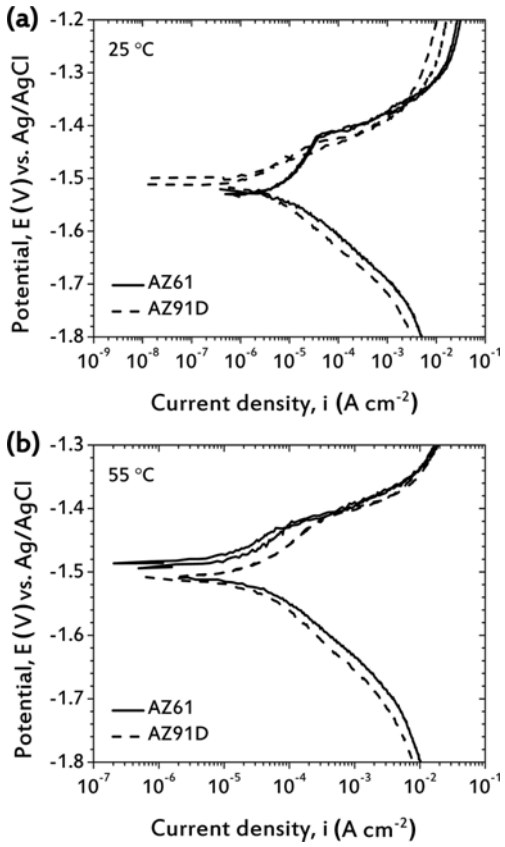

Fig. 3. Variation in (a) corrosion potential (E_{corr}) and potential at 1 mA cm^{-2} and (b) corrosion current density (i_{corr}) of AZ61 and AZ91D as functions of electrolyte temperature in 0.1 M NaCl, as estimated from potentiodynamic tests. The i_{corr} was estimated by the extrapolation of cathodic Tafel slopes to the E_{corr}.

3.2. Potentiodynamic polarization behavior

Potentiodynamic polarization tests were carried out to predict the temperature-dependent probability of corrosion of AZ61 and AZ91D in 0.1 M NaCl solution, in the temperature range of 25-55 °C. The hydrogen evolution during polarization under both anodic and cathodic conditions has a complicated effect on the corrosion behavior of Mg alloys. The hydrogen evolution proceeds as $2H_2O + 2e^- \rightarrow H_2 + 2OH^-$. The hydroxyl ions ($OH^-$) during this reaction increase the pH of the electrolyte, which leads to unexpected decrease in the corrosion susceptibility of Mg alloys during anodic polarization time. Moreover, an interesting observation associated with this reaction is that a rate of hydrogen evolution increases with the anodic polarization [22,23]. Therefore, as shown in Fig. 3, the potentiodynamic polarization tests are performed with two specimens of the same alloy, separately in potential ranges of E_{OCP} to +1 V (anodically) and then from E_{OCP}

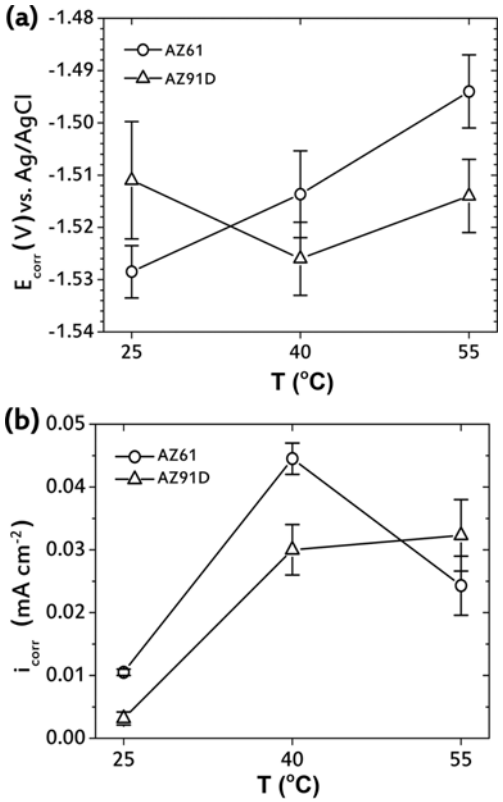

Fig. 4. Anodic and cathodic polarization behaviors of alloys AZ61 and AZ91D with electrolyte temperature in 0.1 M NaCl.

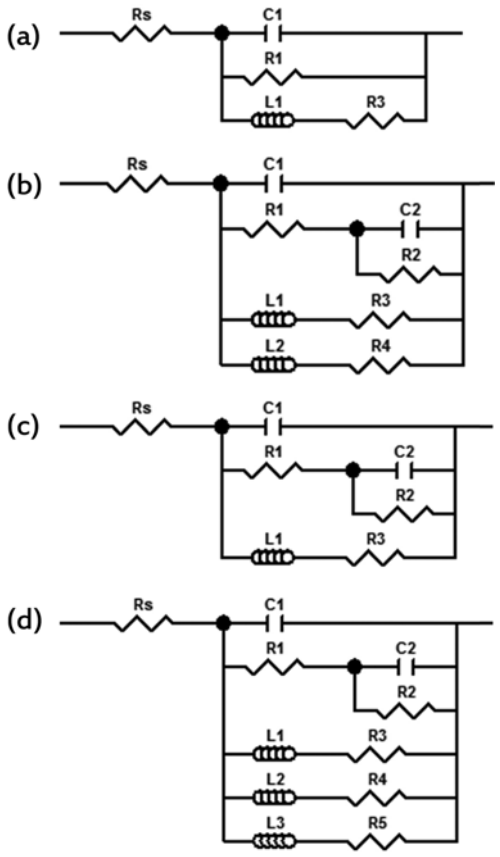

Fig. 5. Equivalent electrical circuit models used at (a, b) open-circuit potential and (c, d) -1.38 $V_{Ag/AgCl}$.

to -1 V (cathodically), to minimize differentiating effect of hydroxyl ions on the polarity.

As evidenced from the results of potentiodynamic tests shown in Fig. 4(a) and 4(b), AZ91D shows higher corrosion potential (E_{corr}) and lower corrosion current density (i_{corr}) than AZ61 at 25 °C. However, it is remarkable that the E_{corr} of AZ61 increased with the electrolyte temperature while that of AZ91D slightly decreased or not changed much. Eventually, alloy AZ61 shows rather higher E_{corr} at 55 °C. Moreover, alloy AZ61 has a lower passivation current density than AZ91D at 55 °C, while their pitting potentials (E_{pit}) exhibit similar values. In addition, the i_{corr} of AZ61 rather decreases at 55 °C, resulting in the lower corrosion rate. These might be explained based on the strengthening of surface passivation associated with the presence of the sub-micron scale particles of β-phase being effectively dispersed within the grains. The lack of reproducibility of i_{corr} measurement for AZ91D might be attributed to the variation of the amount and distribution of α-Mg without any β-phase from place to place.

3.2. Electrochemical impedance behavior

Figure 5 shows equivalent electrical circuit models used in this study. Charge transfer resistance (R_{ct}) is defined as the impedance at intermediate frequency where $-Z_{imag}$ is 0 in Nyquist plots (Figs. 6 and 7). The R_{ct} is a complex function of R1, R2, C1, and C2, but is approximately equal to R1 + R2.

As shown in Fig. 6, the impedance diagrams of the Mg

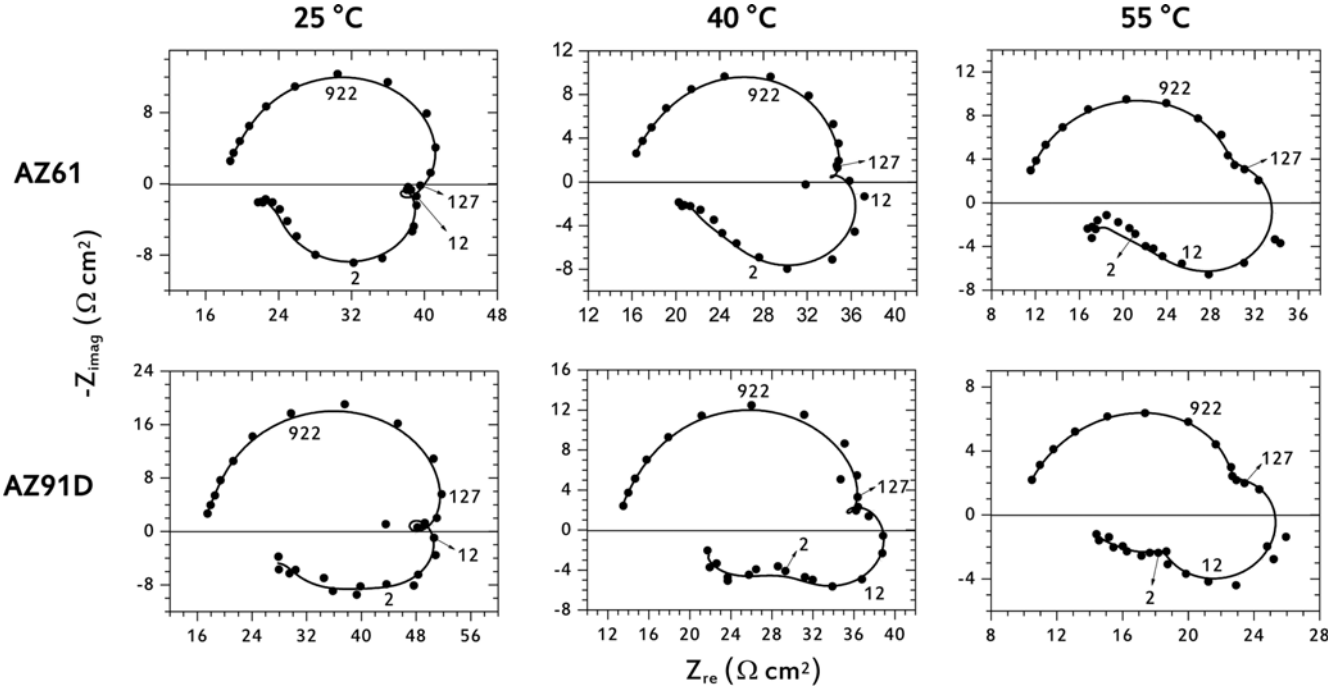

Fig. 6. Nyquist plots of alloys AZ61 and AZ91D measured at applied potential of -1.38 $V_{Ag/AgCl}$ as a function of electrolyte temperature, immediately after immersion in 0.1 M NaCl.

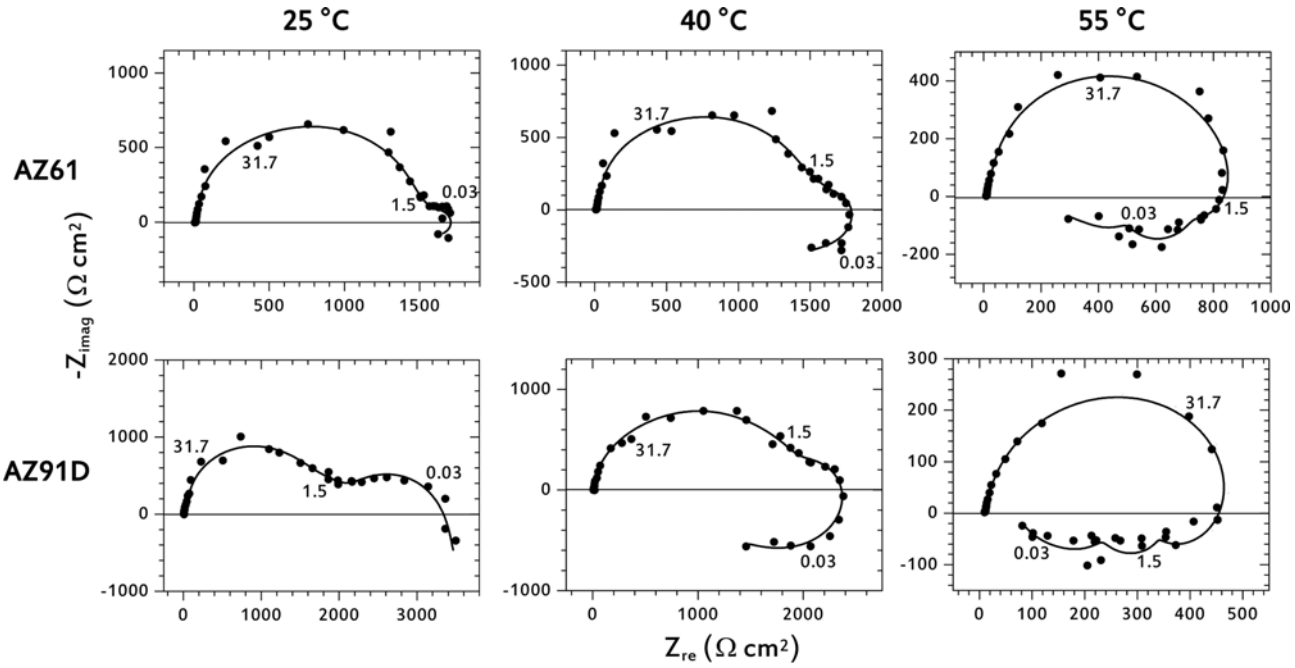

Fig. 7. Nyquist plots of alloys AZ61, and AZ91D measured at open-circuit potential as a function of electrolyte temperature, after immersion for 30 min in 0.1 M NaCl.

alloys AZ61 and AZ91D polarized at -1.38 $V_{Ag/AgCl}$ (anodic domain) at 25 °C afford one well-defined capacitive loop over the high frequency domain. However, for AZ91D, the onset of two inductive loops, extended by the capacitive loop over low frequencies is observed. The origin of the inductive loops in this electrolyte is related to the continuous dissolution on oxide-free surfaces of the Mg alloy [24,25]. The oxide-free areas are considered to be different for each specimen, depending on the area fraction of β-phase. In other words, the presence of α and β phases and their interactions (galvanic action) enlarge the oxide-free area of α-Mg surface, accelerating the initial corrosion rate. Exactly, β-phase has 140-200 mV higher potential than α-Mg matrix [26].

At temperatures higher than 40 °C, however, some part of the inductive loop transforms into a capacitive loop, corresponding to the pre-passivation process [24]. This results in an increase in R_{ct}. Considering that the passivation appears only as the capacitive loop in the impedance diagram, the partial transformation of inductive loop into capacitive loop might imply a manifestation of the corrosion barrier effect of β-phase rather than the galvanic cathode effect to the α-phase.

Similar with above impedance results, an increase in electrolyte temperature leads to decrease in both the high and low frequency capacitive loops when polarized at OCP (Fig. 7). Therefore, some part of the low frequency capacitive loop is transformed to inductive loops, which is accompanied by a decrease in R_{ct}. As mentioned, the expansion of the inductive loop can be explained based on the relaxation of surface coverage due to the corrosion. In case of AZ61 at 55 °C, the first

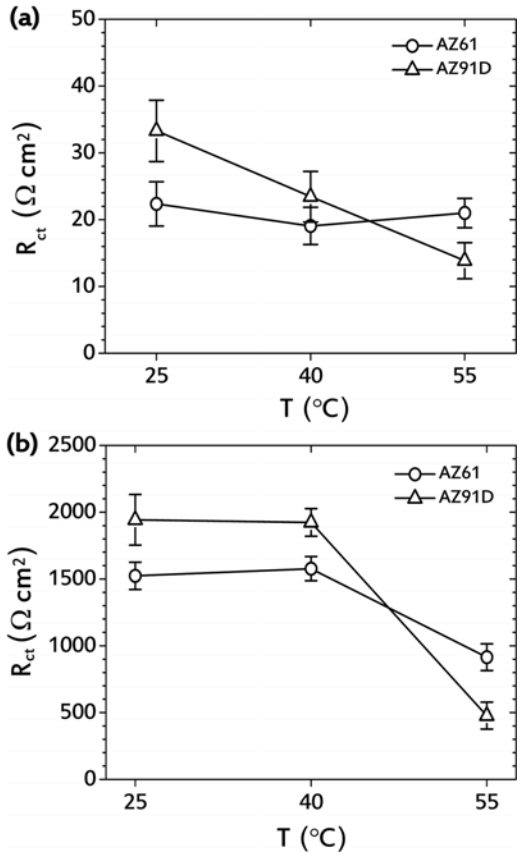

Fig. 8. Variation in charge transfer resistance (R_{ct}) at (a) -1.38 $V_{Ag/AgCl}$, (b) open-circuit potential, as a function of electrolyte temperature, estimated from Fig. 6 and Fig. 7, respectively.

inductive loop occurs at a relatively lower frequency than AZ91D, and exhibits higher value of R_{ct}. In addition, the rapid emergence of inductive loop also leads to an increase in the number of inductive loops in AZ91D, representing a high degradation rate of the electrode surface.

As shown in Fig. 8(a), the R_{ct} of AZ61 maintained at almost a constant value with increase in electrolyte temperature up to 55 °C. On the other hand, the R_{ct} of AZ91D gradually decreases with increase in electrolyte temperature. As a result, AZ61 affords rather higher R_{ct} (21.0 Ω cm^2) than AZ91D (13.9 Ω cm^2) at 55 °C, indicating that the degradation of AZ61 under high temperature is relatively impeded. The gradual decrease in R_{ct} for AZ91D with electrolyte temperature might have resulted from the film breakdown and subsequent corrosion on the α-phase surface without any β-phase during the initial anodic polarization. These experimental results are definitely consistent with those of impedance measurements at OCP after prior immersion for 30 min (Fig. 8b).

3.3. Current transient behavior

Potentiostatic tests were carried out to analyze the kinetics of pitting corrosion in Mg alloys with electrolyte temperature. As shown in Fig. 9, a continuous increase of pitting current with short incubation time (t_i) was observed when the coupons were polarized at -1.38 $V_{Ag/AgCl}$ which value is higher than their E_{pit}. The t_i is the time required for pitting initiation. In most cases, the passive film breakdown occurs more easily above E_{pit} in the presence of Cl^- anions and results in a local exposure of oxide-free area to the corrosive environment. Therefore, a large value of ΔE (= E_{app} - E_{pit}) leads to the convergence of t_i to zero, according to the following Eq. [27]:

$$t_i \propto \exp\left(-\frac{xF\alpha\Delta E}{2RT}\right) \quad (5)$$

where x is the negative charges, F is the Faraday's constant, R is the gas constant, T is the temperature, α is the potential drop at the film/solution interface.

This equation well describes that t_i is a function of ΔE in an electrolyte, where the Cl^- concentration is fixed. The results imply that ΔE is quite large for Mg alloys, so that the experimental condition might be considerably aggressive to corrosion. Hence, the pitting current began to rise sharply with time, reaching the maximum value of current density (i_{max}) within few minutes, with the onset of visible pits. The pitting current of AZ61 increased at the slowest pace with time (i.e. lowest slope) for all the temperature ranges considered in this study. This indicates that the interaction between Mg and Cl^- is the slowest. The difference in increasing rates of current density was more distinct at high temperatures. The convergence of t_i to almost zero and relatively high transient currents during initial immersion at high electrolyte temperature demonstrates that the initial rates of passive film breakdown and pitting propagation is more severe in AZ91D than in AZ61.

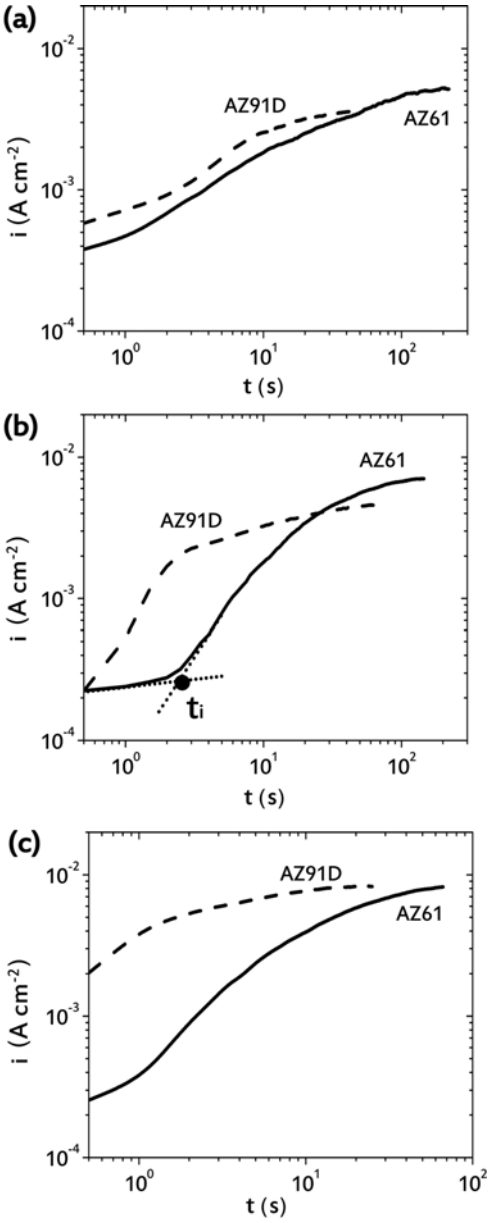

Fig. 9. Corrosion current transients as a function of electrolyte temperature at -1.38 $V_{Ag/AgCl}$ in 0.1 M NaCl: (a) 25 °C, (b) 40 °C, and (c) 55 °C.

Furthermore, the corrosion behavior of the AZ-type Mg alloys during CCT, which is composed of salt spray, drying, and wet steps, was analyzed by measuring the current transients by means of a zero resistance ammeter (Fig. 10). During first 1 h of salt spray, currents were nearly zero due to passivation or inadequacy of electrolyte levels on the electrode surfaces. After 1 h of salt spray, the current abruptly increased for all electrodes, as a result of pit initiation and propagation. From a previous report, the effect of temperature is known to more significant than that of [Cl^-] concentration during the salt spray [8]. During the initial drying period of both

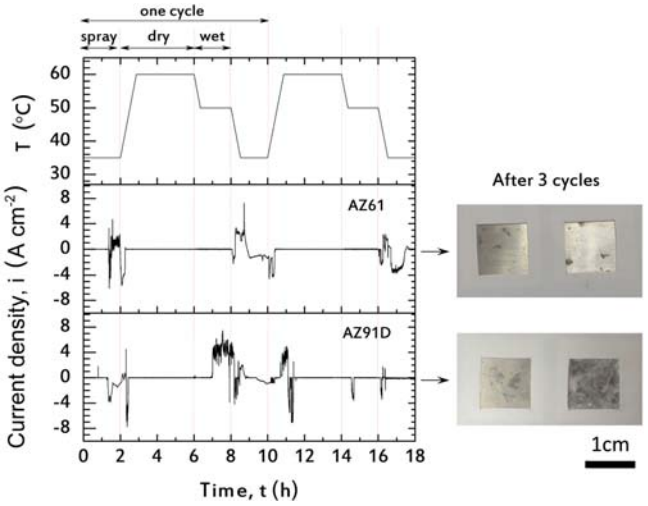

Fig. 10. Corrosion current transients of AZ61 and AZ91D during cyclic corrosion test. The positive and negative current values reflect the corrosion mainly on the WE1 (connected to working electrode) and WE2 (connected to counter electrode) during the tests, respectively.

AZ61 and AZ91D, the current values were almost similar (or just slightly increased), as compared to those under salt spray period.

After the water was dried up completely, the current values abruptly decreased to a nearly zero value again, thereby repassivating the surfaces. This indicates that the electrochemical corrosion stops for all electrodes. However, the wet stage provides water and promotes the progress of cathodic reaction, which leads to corrosion. The main cathodic reaction in neutral aqueous solution is water reduction reaction. The dissolved salts facilitate initiation and propagation of pits more actively in wet stage than in salt spray stage. The high corrosivity of the wet stage might be attributed to the high electrolyte temperature (50 °C) and the presence of concentrated Cl^- ions within the pits. However, only a small current flows through the AZ61 electrodes during the wet period. This result is consistent with that of another our cyclic corrosion tests, except for minor variations. In any case, the results obtained for AZ61 during the wet period were always lower than those of AZ91D. After the first cycle, the currents gradually decreased throughout the entire step, especially for AZ61 and AZ91D electrodes, probably due to the build-up of corrosion by-products.

In general, the higher the content of Al as an alloying element, the lower the corrosion susceptibility of the Mg alloys. Intriguingly, at temperatures higher than 40 °C, AZ91D with the highest Al content revealed lower corrosion resistance when compared to that of AZ61. On the other hand, at room temperature, the corrosion resistance of AZ91D was superior to that of AZ61. Meanwhile, several authors have demonstrated that AZ91D suffers from a similar or higher corrosion attack compared to AZ61 and AZ80 under prolonged exposure conditions, typically for more than 24 days [8-10]. These suggest that the corrosion behavior of AZ-type Mg alloys has a dependency on their morphology and microstructure [10,28,29].

4. CONCLUSIONS

The presence of sub-micron β-phase particles dispersed within the grains of AZ61 affords rather higher E_{corr} and lower i_{corr} at 55 °C than AZ91D, resulting from the strengthening of surface passivation. Moreover, AZ61 shows higher polarization resistance both at open circuit potential and -1.38 $V_{Ag/AgCl}$ (transpassive state), indicating that the film breakdown and subsequent corrosion over the entire surface of AZ61 is relatively impeded. In addition, the pitting current on AZ61 increased at the slowest pace with time when polarized at -1.38 $V_{Ag/AgCl}$ and it was predominant especially at 55 °C. In consequence, only a small current flowed through the AZ61 during the wet period of cyclic corrosion test (50 °C). On the other hand, AZ91D has many α-Mg that do not involving any β-phases, and therefore, the oxide-free area on the α-Mg surface can be enlarged by the galvanic reaction during the initial corrosion measurements.

REFERENCES

1. G. Cole, Eds. J. Quinn, E. Hetrick, and S. Bairley, *Southfield*, MI: USAMP (2006).
2. B. D. Lee, E. J. Kim, U. H. Baek, and J. W. Han, *Met. Mater. Int.* **19**, 135 (2013).
3. Y. H. Kim and W. J. Kim, *Met. Mater. Int.* **21**, 374 (2015).
4. J. Chen, J. Wang, E. H. Han, and W. Ke, *Corros. Sci.* **51**, 477 (2009).
5. L. Wang, T. Shinohara, and B. P. Zhang, *Mater. Des.* **33**, 345 (2012).
6. C. A. Walton, H. J. Martin, M. F. Horstemeyer, and P. T. Wang, *Corros. Sci.* **56**, 194 (2012).
7. G. Song and S. Atrens, *Adv. Eng. Mater.* **1**, 11 (1999).
8. M. C. Merino, A. Pardo, R. Arrabal, S. Merino, P. Sasajus, and M. Mohedano, *Corros. Sci.* **52**, 1696 (2010).
9. Z. Wen, C. Wu, C. Dai, and F. Yang, *J. Alloys Compd.* **488**, 392 (2009).
10. A. Pardo, M. C. Merino, A. E. Coy, F. Viejo, R. Arrabal, and S. Feliú Jr., *Electrochim. Acta* **53**, 7890 (2008).
11. R. K. S. Raman, *Metal. Mater. Trans. A* **35**, 2525 (2004).
12. A. Samaniego, I. Llorente, and S. Feliu Jr., *Corros. Sci.* **68**, 66 (2013).
13. M. Jönsson and D. Persson, *Corros. Sci.* **52**, 1077 (2010).
14. A. Pardo, M. C. Merino, A. E. Coy, R. Arrabal, F. Viejo, and E. Matykina, *Corros. Sci.* **50**, 823 (2008).
15. S. Feliu Jr., C. Maffiotte, J. C. Galván, and V. Barranco, *Corros. Sci.* **53**, 1865 (2011).
16. G. Song, A. Atrens, Z. Wu, and B. Zhang, *Corros. Sci.* **40**, 1769 (1998).

17. A. F. Froats, T.Kr. Aune, D. Hawke, W. Unsworth, J. Hillis, *Metals Handbook*, p.740, Vol.13, 9th ed., Corrosion ASM International, Materials Park, OH (1987).
18. R. P. Vera Cruz, A. Nishikata, and T. Tsuru, *Corros. Sci.* **40**, 125 (1998).
19. W. J. Beom, K. S. Yun, C. J. Park, H. J. Ryu, and Y. H. Kim, *Corros. Sci.* **52**, 734 (2010).
20. G. S. Frankel, *J. Electrochem. Soc.* **145**, 2186 (1998).
21. D. W. Buzza and R. C. Alkire, *J. Electrochem. Soc.* **142**, 1104 (1995).
22. A. Atrens and W. Dietzel, *Adv. Eng. Mater.* **9**, 292 (2007).
23. G. S. Frankel, A. Samaniego, and N. Birbilis, *Corros. Sci.* **70**, 104 (2013).
24. M. Keddam, O. R. Mottos, and H. Takenouti, *J. Electrochem. Soc.* **128**, 257 (1981).
25. H. Schweikert, W. J. Lorenz, and H. Friedburg, *J. Electrochem. Soc.* **127**, 1693 (1980).
26. I. Apachitei, L. E. Fratila-Apachitei, and J. Duszczyk, *Scripta Mater.* **57**, 1012 (2007).
27. L. F. Lin, C. Y. Chao, and D. D. Macdonald, *J. Electrochem. Soc.* **128**, 1194 (1981).
28. T. Zhang, Y. Li, and F. Wang, *Corros. Sci.* **48**, 1249 (2006).
29. G. Song and A. Atrens, *Adv. Eng. Mater.* **5**, 837 (2003).